

Article

Critical Current Density and Vortex Dynamics in Pristine and Irradiated $\text{KCa}_2\text{Fe}_4\text{As}_4\text{F}_2$

Sunseng Pyon ^{1,*}, Soichi Taya ¹, Yuto Kobayashi ¹, Ayumu Takahashi ¹, Wenjie Li ¹, Toshihiro Taen ², Teng Wang ³, Gang Mu ⁴, Hisashi Kitamura ⁵, Ataru Ichinose ⁵ and Tsuyoshi Tamegai ¹

¹ Department of Applied Physics, The University of Tokyo, 7-3-1 Hongo, Bunkyo-ku, Tokyo 113-8656, Japan; taya@issp.u-tokyo.ac.jp (S.T.); momiji3.momo3.keyaki3@gmail.com (Y.K.); naotoshikazuto@gmail.com (A.T.); liwenjie@g.ecc.u-tokyo.ac.jp (W.L.); tamegai@ap.t.u-tokyo.ac.jp (T.T.)

² Institute for Solid State Physics, The University of Tokyo, Kashiwa 277-8581, Japan; taen@issp.u-tokyo.ac.jp

³ State Key Laboratory of Functional Materials for Informatics, Shanghai Institute of Microsystem and Information Technology, Chinese Academy of Sciences, Shanghai 200050, China; wangteng@mail.sim.ac.cn

⁴ National Institute of Radiological Sciences, National Institutes for Quantum and Radiological Science and Technology, Anagawa, Chiba-shi 263-8555, Japan; mugang@mail.sim.ac.cn

⁵ Central Research Institute of Electric Power Industry, Grid Innovation Research Laboratory, 2-6-1, Nagasaka, Yokosuka-shi 240-0196, Japan; kitamura.hisashi@qst.go.jp (H.K.); ai@criepi.denken.or.jp (A.I.)

* Correspondence: pyon@ap.t.u-tokyo.ac.jp

Abstract: We report the critical current density (J_c) and vortex pinning properties in single crystals of a novel iron-based superconductor (IBS) $\text{KCa}_2\text{Fe}_4\text{As}_4\text{F}_2$ with large J_c in the pristine state, before and after introduction of artificial defects by swift-particle irradiation. The effects of 2.6 GeV U and 3 MeV proton irradiations in $\text{KCa}_2\text{Fe}_4\text{As}_4\text{F}_2$ single crystals on transition temperature T_c and J_c , including its dose dependence, are systematically studied. $J_c \sim 8 \text{ MA/cm}^2$ under a self-field at 2 K in the pristine crystal is strongly enhanced up to 19.4 and 17.5 MA/cm^2 by irradiation of 2.6 GeV U-ions and 3 MeV protons, respectively. Suppression of T_c and dose dependence of J_c in $\text{KCa}_2\text{Fe}_4\text{As}_4\text{F}_2$ is different from that in a representative IBS of $(\text{Ba,K})\text{Fe}_2\text{As}_2$, which can be explained by considering the presence of embedded defects in pristine $\text{KCa}_2\text{Fe}_4\text{As}_4\text{F}_2$. The vortex dynamics in the pristine and proton irradiated $\text{KCa}_2\text{Fe}_4\text{As}_4\text{F}_2$ single crystals are also investigated from the analyses of the field dependence of J_c and the normalized magnetic relaxation rate. In addition to the contribution of embedded defects, weak collective pinning is considered for comprehensive analyses. Vortex dynamics in $\text{KCa}_2\text{Fe}_4\text{As}_4\text{F}_2$ is similar to those in $(\text{Ba,K})\text{Fe}_2\text{As}_2$ to some extent, and different from that in anisotropic $\text{Li}_{0.8}\text{Fe}_{0.2}\text{OHFeSe}$. Large anisotropy, due to the presence of insulating blocking layers in $\text{KCa}_2\text{Fe}_4\text{As}_4\text{F}_2$, which leads to much lower irreversibility field (H_{irr}) compared with 122-type IBSs, strongly affect the vortex dynamics.

Keywords: iron-based superconductors (IBS); vortex dynamics; ion irradiation; $\text{KCa}_2\text{Fe}_4\text{As}_4\text{F}_2$



Citation: Pyon, S.; Taya, S.; Kobayashi, Y.; Takahashi, A.; Li, W.; Taen, T.; Wang, T.; Mu, G.; Kitamura, H.; Ichinose, A.; et al. Critical Current Density and Vortex Dynamics in Pristine and Irradiated $\text{KCa}_2\text{Fe}_4\text{As}_4\text{F}_2$. *Materials* **2021**, *14*, 5283. <https://doi.org/10.3390/ma14185283>

Academic Editor: Pavel Diko

Received: 30 July 2021

Accepted: 10 September 2021

Published: 14 September 2021

Publisher's Note: MDPI stays neutral with regard to jurisdictional claims in published maps and institutional affiliations.



Copyright: © 2021 by the authors. Licensee MDPI, Basel, Switzerland. This article is an open access article distributed under the terms and conditions of the Creative Commons Attribution (CC BY) license (<https://creativecommons.org/licenses/by/4.0/>).

1. Introduction

Iron-based superconductors (IBSs) are attracting a great deal of attention due to their notable features, such as their relatively high transition temperature (T_c), high upper critical field (H_{c2}), and large critical current density (J_c) [1]. In typical IBSs, such as 122-type compound $(\text{Ba,K})\text{Fe}_2\text{As}_2$ [2], electronic states are weakly anisotropic, although their crystal structures are characterized by the presence of two-dimensional FePn (Pn : As, P) or FeCh (Ch : S, Se, Te) layers. This is in contrast to quasi two-dimensional electronic states in cuprate superconductors with two-dimensional CuO_2 layers [3,4]. Recently, however, it was suggested that quasi two-dimensional electronic states emerge in novel IBSs, such as 12442-type compounds [5–9] or some IBSs consisting of FeSe layers sandwiched by thick insulating layers [10,11]. The 12442-type IBSs have double Fe_2As_2 conducting layers between two neighboring Ca_2F_2 insulating layers [5]. Due to the presence of insulating layers, anisotropic electronic states are realized as revealed by the highly anisotropic H_{c2} [12,13]

and torque analyses [14]. $\text{KCa}_2\text{Fe}_4\text{As}_4\text{F}_2$ is the first and a well-studied 12442-type IBS [8] and its anisotropic physical properties have been demonstrated. In $\text{KCa}_2\text{Fe}_4\text{As}_4\text{F}_2$, quasi two-dimensional electronic behavior, which is similar to that of cuprate superconductors, has been revealed by neutron spin resonance [15]. The quasi two-dimensional electronic state was also suggested from the large anisotropy of electrical resistivity, with $\rho_c/\rho_{ab} > 100$, and semiconductor-like ρ_c [16]. Furthermore, a large anisotropy parameter, $\gamma (= H_{c2}^{ab}/H_{c2}^c) \sim 8$, was also evaluated near T_c [12,16]. Notable features of this highly anisotropic $\text{KCa}_2\text{Fe}_4\text{As}_4\text{F}_2$ are moderate T_c of ~ 34 K, and larger J_c , and H_{c2} compared with 122-type IBSs. Large H_{c2}/ab above 700 kOe at low temperatures has been evaluated [17], although the irreversibility field (H_{irr}), which separate zero and finite J_c regions, is relatively low [12,16]. The in-plane J_c evaluated from the measurement of irreversible magnetization at 2 K under the self-field is 8.2 MA/cm^2 , which is significantly larger compared with that of 122-type IBSs [16].

One of the most intriguing topics in $\text{KCa}_2\text{Fe}_4\text{As}_4\text{F}_2$ is how the significantly high J_c is enhanced by adding artificial pinning centers. It is well known that J_c in superconductors, such as cuprates and IBSs, can be enhanced by introducing defects using swift particle irradiations, and significant effects on physical properties, such as remarkable enhancements of J_c by irradiations of heavy ions and protons have been demonstrated [16,18–30]. For $\text{KCa}_2\text{Fe}_4\text{As}_4\text{F}_2$, enhancement of J_c up to 19 MA/cm^2 at 2 K under self-field is also demonstrated by introducing columnar defects in terms of heavy-ion irradiation, although the irradiation dose is limited [16]. It is also well known that introducing point defects by proton irradiation is effective at enhancing J_c in cuprate superconductors [31,32] and IBSs [24,27]. A systematic study of the effect of columnar and point defects on J_c in $\text{KCa}_2\text{Fe}_4\text{As}_4\text{F}_2$ is demanded.

Furthermore, investigation of vortex pinning properties in $\text{KCa}_2\text{Fe}_4\text{As}_4\text{F}_2$ is also required to understand its J_c behavior. It is needless to say that vortex dynamics is one of the central issues related, not only to basic solid-state physics, but also to applications. Vortex dynamics in cuprates have been extensively studied in past decades [33,34]. When the c -axis coherence length, ξ_c , is larger than the layer distance, d , such as in $\text{YBa}_2\text{Cu}_3\text{O}_7$, the magnetic field generates well-connected quantized vortices via interlayer coupling, which creep collectively when the thermal energy is stronger than the pinning energy [33,34]. On the other hand, when the interlayer coupling is very weak, with $\xi_c < d$, such as in $\text{Bi}_2\text{Sr}_2\text{CuCa}_2\text{O}_{8+y}$, quantized vortices can be considered as stacks of pancake vortices, which can creep individually in each layer [33,34]. These results suggest that anisotropic crystal structure and electronic structure strongly affect the behavior of vortices. Vortex dynamics in IBSs has also been studied by comparing them with those in cuprate superconductors. For analyses of vortex dynamics, magnetic relaxation in clean single crystals, where a critical state is realized in the whole sample, has been utilized since transport measurements are challenging due to the extremely large J_c . Up to now, 122-type compounds, such as $(\text{Ba,K})\text{Fe}_2\text{As}_2$ or $\text{Ba}(\text{Fe,Co})_2\text{As}_2$, and 11-type compounds, such as $\text{Fe}(\text{Te,Se})$ and FeSe , have mainly been studied [24,27,35,36]. In these weakly anisotropic materials with an anisotropy parameter 2–3, vortex pinning properties have been interpreted in either weak-collective pinning or strong pinning scenarios [1,2,24,27,35]. On the other hand, in one of IBSs, $\text{Li}_{0.8}\text{Fe}_{0.2}\text{OHFeSe}$, with a highly anisotropic crystal structure, breakdown of conventional creep theory has been pointed out [37]. To understand general characteristics of vortex pinning in anisotropic high temperature superconductors, including cuprates and IBSs, further investigation of vortex dynamics in anisotropic materials, such as $\text{KCa}_2\text{Fe}_4\text{As}_4\text{F}_2$, is demanded.

In this study, we investigated the effect of columnar defects and point defects created by irradiation of U ions and protons in $\text{KCa}_2\text{Fe}_4\text{As}_4\text{F}_2$ single crystals. Changes in T_c and J_c were systematically studied as a function of the irradiation dose. We also investigated the vortex pinning properties and the vortex dynamics in $\text{KCa}_2\text{Fe}_4\text{As}_4\text{F}_2$ before and after the introduction of point defects. A part of the data of $\text{KCa}_2\text{Fe}_4\text{As}_4\text{F}_2$ were compared to those

of $(\text{Ba,K})\text{Fe}_2\text{As}_2$, which belong to 122-type IBSs and is a representative IBS, and those of $\text{Li}_{0.8}\text{Fe}_{0.2}\text{OHFeSe}$, which has anisotropic crystal structure similar to $\text{KCa}_2\text{Fe}_4\text{As}_4\text{F}_2$.

2. Experimental Methods

Single crystals of $\text{KCa}_2\text{Fe}_4\text{As}_4\text{F}_2$ were grown using the self-flux method with KAs as the flux. Details of sample growth and the basic physical properties are reported in Reference [12]. $\text{Ba}_{0.6}\text{K}_{0.4}\text{Fe}_2\text{As}_2$ single crystals, which were used as reference materials to be compared with $\text{KCa}_2\text{Fe}_4\text{As}_4\text{F}_2$, were also synthesized using the FeAs self-flux method [27,38]. The 2.6 GeV U ions were irradiated parallel to the c -axis at room temperature at RIKEN Ring Cyclotron in RI Beam Factory, operated by RIKEN Nishina Center and CNS, the University of Tokyo. The irradiation dose was evaluated using the dose-equivalent magnetic field called the “matching field”, at which all defects are occupied by single vortices, $B_\Phi = n\Phi_0$. Here, n is the areal density of CDs and Φ_0 is a flux quantum. The 3 MeV protons were irradiated parallel to the c -axis at room temperature at the National Institute of Radiological Sciences Heavy Ion Medical Accelerator in Chiba, Japan (NIRS-HIMAC). Cross-sectional observations of the single crystals were performed with a scanning transmission electron microscope (STEM) (JEOL, JEM-2100F, Akishima, Tokyo, Japan). The spatial resolution of the JEOL JEM-2100F microscope was 0.2 nm; however, we set it as 0.5 nm to add contrast to the STEM image. The specimens for STEM were prepared by digging and milling using a focused-ion beam (FIB), which is called the microsampling technique. Final milling using FIB was conducted at an acceleration voltage of 30 kV and with a very weak ion current of ~ 10 pA without tilting the specimen. Magnetization was measured in a commercial superconducting quantum interference device magnetometer (MPMS-XL5, Quantum Design, San Diego, CA, United States) with an applied magnetic field parallel to the c -axis. In this system, temperature accuracy was $\pm 1\%$, and magnetic field resolutions were 0.1 G up to 5 kOe and 1 G up to 50 kOe.

3. Experimental Results and Discussions

In this section, first, the effects of 2.6 GeV U and 3 MeV proton irradiations on T_c and J_c estimated from magnetization measurements in $\text{KCa}_2\text{Fe}_4\text{As}_4\text{F}_2$ are discussed. STEM images of both the pristine and 2.6-GeV U-irradiated $\text{KCa}_2\text{Fe}_4\text{As}_4\text{F}_2$ are also presented. Second, the vortex dynamics of the pristine and 3 MeV proton irradiated crystals are discussed based on magnetization measurements and analyses of magnetic relaxation.

3.1. Effects of 2.6 GeV U and 3 MeV Proton Irradiations on T_c and J_c in $\text{KCa}_2\text{Fe}_4\text{As}_4\text{F}_2$

First, STEM analyses of the pristine and 2.6-GeV U ion-irradiated $\text{KCa}_2\text{Fe}_4\text{As}_4\text{F}_2$ crystals with an electron beam injected along a -axis were performed. As shown in the STEM images in Figure 1a,b, some black lines parallel to the ab -plane were observed in both pristine and U-irradiated $\text{KCa}_2\text{Fe}_4\text{As}_4\text{F}_2$. Although the existence of these sparsely distributed defects cannot explain the significantly larger J_c in pristine $\text{KCa}_2\text{Fe}_4\text{As}_4\text{F}_2$, they suggest the presence of atomic scale defects or chemical inhomogeneities, which may have contributed as pinning centers. In the 2.6-GeV U-irradiated $\text{KCa}_2\text{Fe}_4\text{As}_4\text{F}_2$, clear columnar defects with a diameter ~ 5 nm along the c -axis were observed, which were similar to the case of $\text{Ba}(\text{Fe,Co})_2\text{As}_2$ and $(\text{Ba,K})\text{Fe}_2\text{As}_2$ [20,23,39].

Next, the effects of columnar defects on T_c and J_c in $\text{KCa}_2\text{Fe}_4\text{As}_4\text{F}_2$ were investigated. Figure 2a shows zero-field-cooled magnetization measurements with a $H//c$ -axis for 2.6-GeV U-irradiated $\text{KCa}_2\text{Fe}_4\text{As}_4\text{F}_2$. It is clear that the onset of superconductivity is systematically suppressed by increasing B_Φ . Normalized T_c estimated from the linear extrapolation from the low temperature is summarized in Figure 2b. The B_Φ dependence of T_c is also shown in the inset of Figure 2b. For comparison, the B_Φ dependence of T_c for $(\text{Ba,K})\text{Fe}_2\text{As}_2$ are also shown [26]. T_c of both $\text{KCa}_2\text{Fe}_4\text{As}_4\text{F}_2$ and $(\text{Ba,K})\text{Fe}_2\text{As}_2$ are monotonically decreased with increasing B_Φ , although B_Φ dependence of T_c in $\text{KCa}_2\text{Fe}_4\text{As}_4\text{F}_2$ is stronger than that of $(\text{Ba,K})\text{Fe}_2\text{As}_2$. The rate of the reduction of the normalized T_c estimated from Figure 2b is 0.3%/T and 0.9%/T for $(\text{Ba,K})\text{Fe}_2\text{As}_2$ and $\text{KCa}_2\text{Fe}_4\text{As}_4\text{F}_2$, respectively.

If columnar defects only destroy local superconductivity, T_c should not be affected by introducing such defects. The suppression of T_c can be explained by considering the effect of point defects created by secondary electrons, which are generated via interaction with highly energetic U ions and the lattice [26]. It is known that magnetic impurities lead to suppression of T_c in *s*-wave superconductors, as discussed by Abrikosov and Gor'kov [40], and point defects may work similar to magnetic impurities in anisotropic $\text{KCa}_2\text{Fe}_4\text{As}_4\text{F}_2$. Unfortunately, however, it is not easy to estimate the dose and energy of such secondary electrons in a given material.

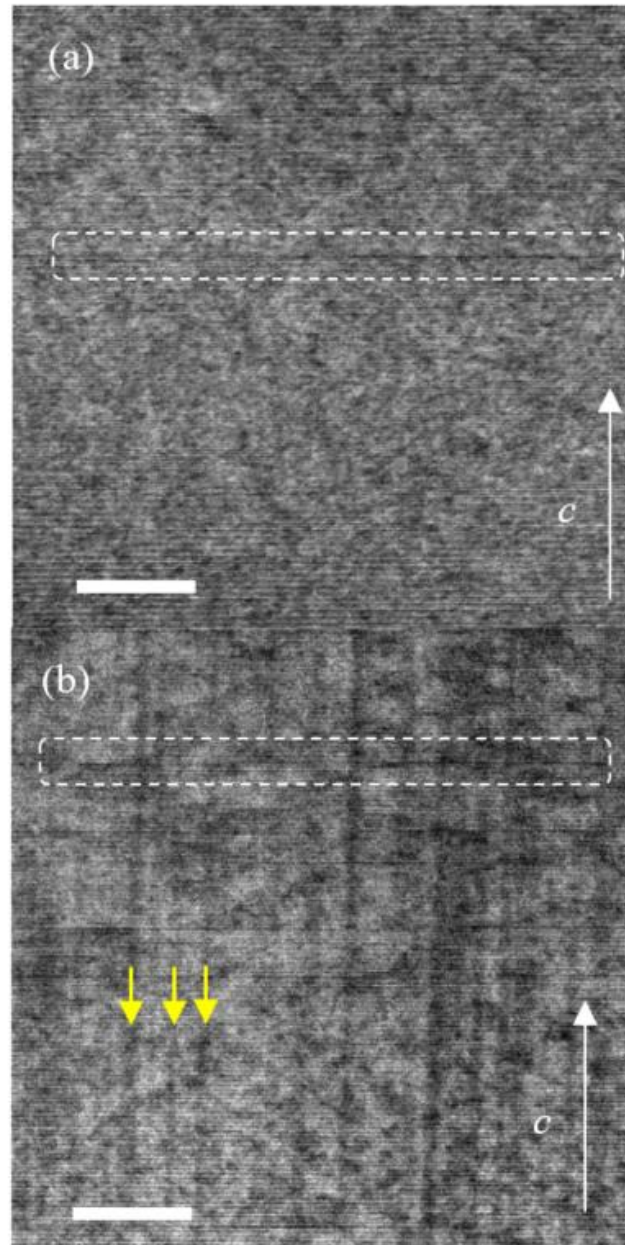


Figure 1. STEM images of (a) the pristine and (b) 2.6-GeV U-irradiated $\text{KCa}_2\text{Fe}_4\text{As}_4\text{F}_2$ for an electron beam injected along the *a* axis. Scale bars in (a,b) correspond to 50 nm. Broken squares in (a,b) emphasize the location of horizontal black lines in STEM images, which we interpreted to be thin planar defects. Yellow arrows in (b) show examples of columnar defects generated by 2.6-GeV U-irradiation.

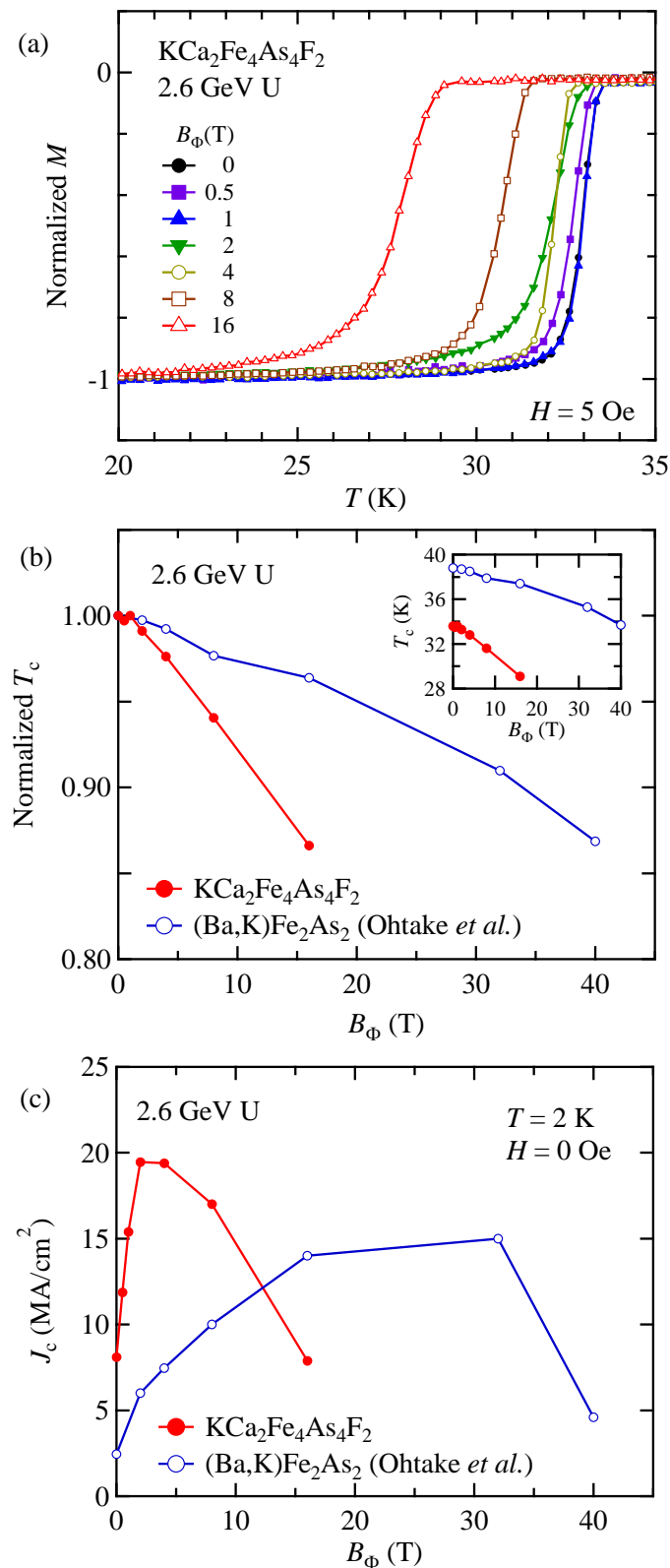


Figure 2. (a) Temperature dependence of normalized magnetization of 2.6 GeV U-irradiated $\text{KCa}_2\text{Fe}_4\text{As}_4\text{F}_2$ with various B_Φ at 5 Oe. The irradiation dose is evaluated by B_Φ . The B_Φ dependence of (b) normalized T_c and (c) J_c at 2 K under self-field in 2.6 GeV U-irradiated $\text{KCa}_2\text{Fe}_4\text{As}_4\text{F}_2$ and $(\text{Ba,K})\text{Fe}_2\text{As}_2$ [26]. The B_Φ dependence of T_c is also shown in the inset of (b).

Next, the in-plane J_c for $H//c$ -axis in $\text{KCa}_2\text{Fe}_4\text{As}_4\text{F}_2$ is evaluated by measuring the irreversible magnetization using the extended Bean model [20,41,42],

$$J_c [\text{A}/\text{cm}^2] = 20\Delta M/a(1 - a/3b) \quad (1)$$

where ΔM [emu/cm^3] is $M_{\text{down}} - M_{\text{up}}$. M_{up} and M_{down} are the magnetization when sweeping the field up and down, respectively, and a [cm] and b [cm] are the sample width and length ($a < b$). Figure 2c shows the B_Φ dependence of J_c in $\text{KCa}_2\text{Fe}_4\text{As}_4\text{F}_2$ irradiated with 2.6 GeV U ions at $T = 2$ K under the self-field. For comparison, similar data for a $(\text{Ba,K})\text{Fe}_2\text{As}_2$ single crystal are also shown [26]. The B_Φ dependence of J_c in $\text{KCa}_2\text{Fe}_4\text{As}_4\text{F}_2$ shows similar trends to that of $(\text{Ba,K})\text{Fe}_2\text{As}_2$, although the B_Φ for the largest J_c are quite different. In the low B_Φ region, J_c is enhanced in proportion to $B_\Phi^{-1/2}$. This can be understood by a simple estimation based on half-loop excitations of vortices in the matrix of discontinuous columnar defects [26]. By increasing B_Φ further, J_c takes a maximum at a certain B_Φ , and it starts to decline above this value. The maximum J_c of $19.4 \text{ MA}/\text{cm}^2$ is realized in $\text{KCa}_2\text{Fe}_4\text{As}_4\text{F}_2$ with $B_\Phi = 2$ T, and that of $15 \text{ MA}/\text{cm}^2$ is realized in $(\text{Ba,K})\text{Fe}_2\text{As}_2$ with $B_\Phi = 32$ T. This value is more than twice as large as that of J_c of the pristine sample, and larger than that of irradiated $(\text{Ba,K})\text{Fe}_2\text{As}_2 \sim 15 \text{ MA}/\text{cm}^2$, as shown in Figure 2c [26]. The J_c in $\text{KCa}_2\text{Fe}_4\text{As}_4\text{F}_2$ starts to decline above $B_\Phi = 4$ T, which is much earlier than that in $(\text{Ba,K})\text{Fe}_2\text{As}_2$, as shown in Figure 2c. This early J_c suppression at a smaller B_Φ is consistent with stronger suppression of T_c , which could be due to stronger generation of secondary electrons, as discussed above.

Following the effect of columnar defects, the effects of point defects on T_c and J_c in $\text{KCa}_2\text{Fe}_4\text{As}_4\text{F}_2$ were investigated. Similar to the case of columnar defects, the onset of superconductivity was systematically suppressed by increasing dose, as shown in Figure 3a. Figure 3b shows the dose dependence of normalized T_c in 3 MeV proton irradiated $\text{KCa}_2\text{Fe}_4\text{As}_4\text{F}_2$. The dose dependence of T_c is also shown in the inset of Figure 3b. For comparison, the dose dependence of T_c for $(\text{Ba,K})\text{Fe}_2\text{As}_2$ is also shown in Figure 3b and in its inset [43]. The T_c of both $\text{KCa}_2\text{Fe}_4\text{As}_4\text{F}_2$ and $(\text{Ba,K})\text{Fe}_2\text{As}_2$ monotonically decrease with increasing proton dose. It should be noted that the rate of T_c reduction in both $\text{KCa}_2\text{Fe}_4\text{As}_4\text{F}_2$ and $(\text{Ba,K})\text{Fe}_2\text{As}_2$ estimated from Figure 3b are 0.9 and 1.0% per 1×10^{16} ions/ cm^2 , respectively. These results suggest that the density of created point defects by proton irradiation and their effects on T_c is similar in $\text{KCa}_2\text{Fe}_4\text{As}_4\text{F}_2$ and $(\text{Ba,K})\text{Fe}_2\text{As}_2$. This is in contrast to the case of 2.6-GeV U-irradiated $\text{KCa}_2\text{Fe}_4\text{As}_4\text{F}_2$ and $(\text{Ba,K})\text{Fe}_2\text{As}_2$, where the amount of point defects generated by secondary electrons may depend on the material. Figure 3c show the dose dependence of J_c in $\text{KCa}_2\text{Fe}_4\text{As}_4\text{F}_2$ irradiated with 3 MeV proton at $T = 2$ K under a self-field. For comparison, similar data for $(\text{Ba,K})\text{Fe}_2\text{As}_2$ measured at $H = 1$ kOe are also shown. J_c in $\text{KCa}_2\text{Fe}_4\text{As}_4\text{F}_2$ reaches its maximum of $17.5 \text{ MA}/\text{cm}^2$ at a dose of 3×10^{16} ions/ cm^2 . On the other hand, J_c of $(\text{Ba,K})\text{Fe}_2\text{As}_2$ reaches its maximum of $14 \text{ MA}/\text{cm}^2$ at a dose of 5×10^{16} ions/ cm^2 . The doses for maximum J_c are similar, although that of $\text{KCa}_2\text{Fe}_4\text{As}_4\text{F}_2$ is a little smaller. Such a difference can be explained by the fact that the pristine $\text{KCa}_2\text{Fe}_4\text{As}_4\text{F}_2$ contains embedded point defects, which are atomic-scale defects due to strains or chemical inhomogeneities, and are responsible for high J_c by working as pinning centers [16]. As discussed above, suppression of T_c and the dose dependence of J_c in 2.6-GeV U-ion or 3 MeV proton-irradiated $\text{KCa}_2\text{Fe}_4\text{As}_4\text{F}_2$ are different from those in typical IBS of $(\text{Ba,K})\text{Fe}_2\text{As}_2$, which can be explained by considering the embedded defects in pristine $\text{KCa}_2\text{Fe}_4\text{As}_4\text{F}_2$. It should be emphasized that maximum J_c in $\text{KCa}_2\text{Fe}_4\text{As}_4\text{F}_2$ is larger than that in 122 compounds, which have been extensively studied as raw materials for wires and tapes for future high-field applications [44–46]. Fabrications of wires and tapes of $\text{KCa}_2\text{Fe}_4\text{As}_4\text{F}_2$ are demanded.

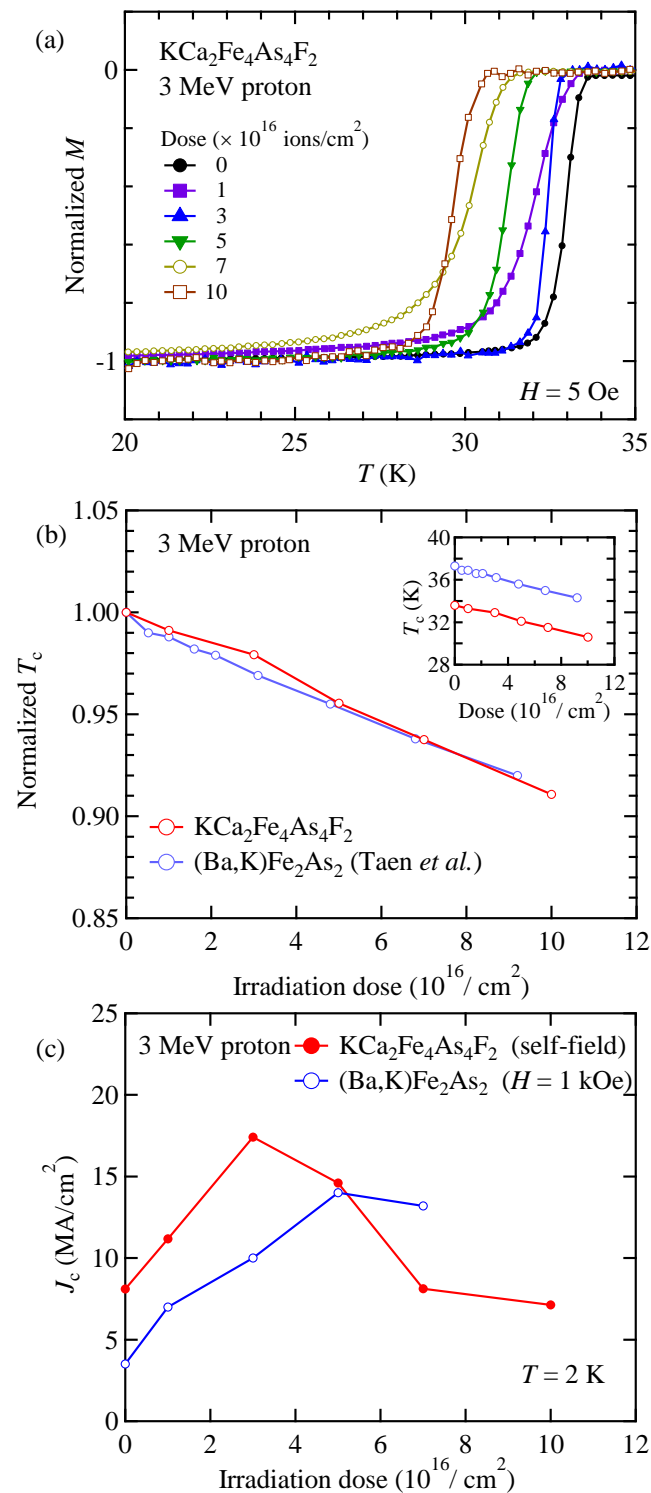


Figure 3. (a) Temperature dependence of normalized magnetization of 3 MeV proton irradiated $\text{KCa}_2\text{Fe}_4\text{As}_4\text{F}_2$ with various dose at 5 Oe. (b) Dose dependence of normalized T_c in 3 MeV proton irradiated $\text{KCa}_2\text{Fe}_4\text{As}_4\text{F}_2$ and $(\text{Ba,K})\text{Fe}_2\text{As}_2$ [27]. Dose dependence of T_c is also shown in the inset of (b). (c) Dose dependence of J_c at 2 K in 3 MeV proton irradiated $\text{KCa}_2\text{Fe}_4\text{As}_4\text{F}_2$ at self-field and $(\text{Ba,K})\text{Fe}_2\text{As}_2$ at $H = 1$ kOe.

3.2. Vortex Dynamics in Pristine and Proton Irradiated $\text{KCa}_2\text{Fe}_4\text{As}_4\text{F}_2$

Figure 4a shows magnetic field dependence of J_c for $H // c$ at various temperatures in the pristine $\text{KCa}_2\text{Fe}_4\text{As}_4\text{F}_2$. At all temperatures, J_c monotonically decreases with mag-

netic field. These features are similar to those in optimally-doped (Ba,K)Fe₂As₂ [27] and Li_{0.8}Fe_{0.2}OHFeSe [37]. By contrast, a broad peaks in J_c - H curves, sometimes referred to as fish-tail effects, are observed in other IBSs, such as Ba(Fe,Co)₂As₂ [24] and Fe(Te,Se) [35]. One of the possible mechanisms of the fish-tail effect is weak collective pinning, which is attributed to the presence of dense atomic-scale defects [47,48]. The absence of a fish-tail effect in KCa₂Fe₄As₄F₂ is possibly explained by the dominance of strong pinning due to the presence of embedded defects in pristine crystal. Furthermore, at low temperatures below 15 K and above ~10 kOe, J_c shows a power-law decay with the field, $J_c \propto H^{-\alpha}$, with $\alpha \sim 1$. The decay of J_c proportional to H^{-1} is observed in YBa₂Cu₃O₇ with columnar defects, which is explained as follows [19]; for example, at $H = 10$ kOe, the distance between vortices is $(\Phi_0/H)^{1/2} \sim 50$ nm. If the pinning centers are sparse and their average separation is larger than 50 nm, all these pinning centers are occupied by vortices above 10 kOe. Hence above this field, the pinning force F_p will stay constant, in spite of the increase in H . So, the value of J_c will decrease in proportional to H^{-1} , since $F_p = 1/c \cdot J_c H$ [49,50]. In other words, observation of $\alpha \sim 1$ suggests that there are sparse strong pinning centers in the pristine KCa₂Fe₄As₄F₂, which may also explain the exceptionally large J_c at low temperatures in this system. It may also explain the slightly lower T_c in KCa₂Fe₄As₄F₂ compared with (Ba,K)Fe₂As₂ with a similar hole number per Fe. On the other hand, at higher temperatures above 15 K, J_c decreases faster with magnetic field, and no power-law field dependence is observed. Similar behavior is also observed in 3 MeV proton irradiated KCa₂Fe₄As₄F₂, where J_c takes its maximum at a dose of 3×10^{16} ions/cm². As shown in Figure 4b, at low temperatures below 15 K and above ~20 kOe, J_c again shows the power-law decay, $H^{-\alpha}$ with $\alpha \sim 1$. Above 15 K, J_c decreases strongly with the magnetic field. This trend is very similar to that in the pristine sample, although the field dependence of J_c is a little weaker. As shown in Figure 4c, in 3 MeV proton irradiated KCa₂Fe₄As₄F₂ with a dose of 10×10^{16} ions/cm², the power-law field dependence of J_c with smaller α (~1/2) is observed at low temperatures, although such behavior is absent at temperatures above 10 K. With increasing the proton dose, α at low temperatures changes from ~1 to ~1/2. In the case of sparse strong pinning, $\alpha = 1/2$ or $5/9$ is predicted [48,51]. So, the change of α from ~1 to ~1/2 may indicate the change of pinning, from very sparse strong pinning to sparse strong pinning. Vortices in the pristine KCa₂Fe₄As₄F₂ are pinned by embedded defects. After the proton irradiation, the strong pinning of vortices by point defects introduced by proton irradiation becomes dominant. We have reported changes of α from ~1/2 to ~1/3 by creating point defects via proton irradiation in various IBSs [24,27,52,53]. The difference in the field dependence of J_c between KCa₂Fe₄As₄F₂ and other IBSs may be caused by the existence of embedded defects in the pristine KCa₂Fe₄As₄F₂. Another remarkable feature of $M(H)$ is fast decay of J_c at higher temperatures and higher magnetic fields. Such behavior of J_c may be related to highly anisotropic properties in KCa₂Fe₄As₄F₂, which will be discussed below.

Vortex dynamics in the pristine and proton irradiated KCa₂Fe₄As₄F₂ crystal were investigated by measuring the normalized magnetic relaxation rate, $S = |d \ln M(t) / d \ln t|$. The decay of magnetization with time, $M(t)$, due to creep motion of vortices was traced for an hour, after the critical state was prepared. Figure 5a,b show the magnetic field dependence of S at $T = 5, 10,$ and 15 K for $H//c$ in the pristine and 3 MeV proton irradiated KCa₂Fe₄As₄F₂ at a dose of 3×10^{16} ions/cm², respectively. The dimensions of the pristine and proton irradiated samples were $0.0178 \times 0.0212 \times 0.0008$ and $0.0235 \times 0.049 \times 0.0013$ cm³, respectively. There were three notable features in the behavior of S . First, characteristic dip features at low magnetic fields below 10 kOe could be identified in both the pristine and 3 MeV proton irradiated KCa₂Fe₄As₄F₂. The characteristic field for the suppression of S is roughly equal to the self-field $H_{sf} = J_c \cdot t$, as we discussed in Ref. [54], where t is the thickness of the sample, as indicated by arrows. H_{sf} values for the pristine sample were evaluated as 4.7 kOe, 2.0 kOe, and 0.7 kOe at 5 K, 10 K, and 15 K, respectively, while those for the proton-irradiated sample were evaluated as 10.5 kOe, 5.3 kOe, and 2.2 kOe at 5 K, 10 K, and 15 K, respectively. Similar suppressions of S at

low magnetic fields below the self-field have been observed in pristine $\text{Ba}(\text{Fe},\text{Co})_2\text{As}_2$ and $(\text{Ba},\text{K})\text{Fe}_2\text{As}_2$ [24,27]. Second, at high magnetic fields, S in the pristine $\text{KCa}_2\text{Fe}_4\text{As}_4\text{F}_2$ increases rapidly above a temperature dependent characteristic field, although S in the proton-irradiated $\text{KCa}_2\text{Fe}_4\text{As}_4\text{F}_2$ increases monotonically up to 40 kOe. Third, the values of S in $\text{KCa}_2\text{Fe}_4\text{As}_4\text{F}_2$ are larger than those in $(\text{Ba},\text{K})\text{Fe}_2\text{As}_2$ and $\text{Ba}(\text{Fe},\text{Co})_2\text{As}_2$ with values of 0.02–0.03 [24,27].

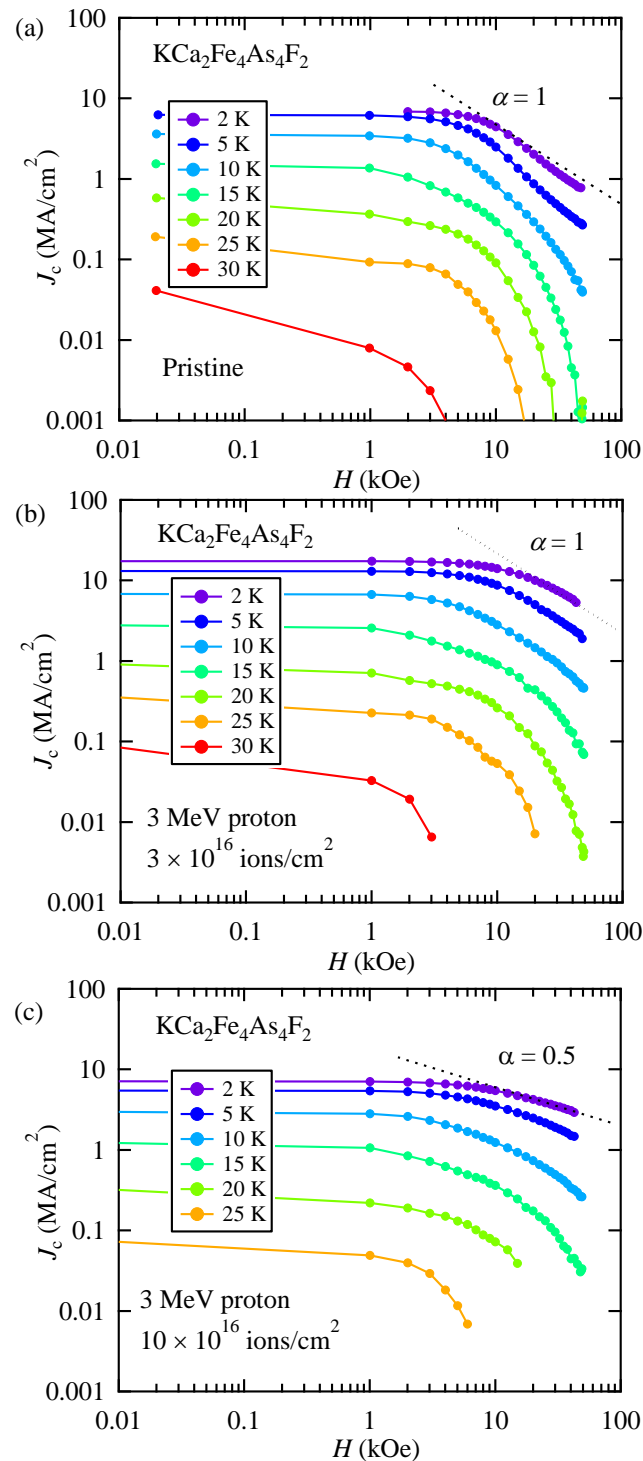


Figure 4. Magnetic field dependence of critical current densities for $H//c$ at various temperatures in (a) the pristine and 3 MeV proton irradiated $\text{KCa}_2\text{Fe}_4\text{As}_4\text{F}_2$ with dose of (b) 3×10^{16} or (c) 10×10^{16} ions/cm².

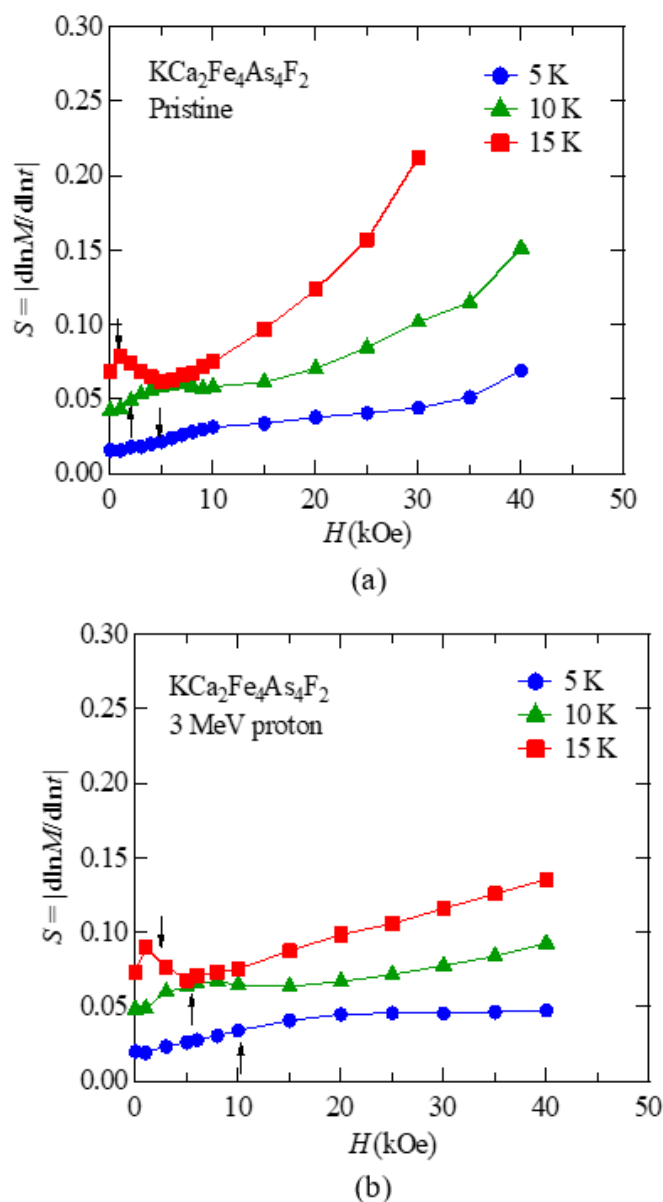


Figure 5. Magnetic field dependence of the normalized magnetic relaxation rate $S = |\ln M(t)/\ln t|$ at $T = 5, 10,$ and 15 K under $H//c$ in (a) the pristine and (b) 3 MeV proton irradiated (3×10^{16} ions/cm²) $\text{KCa}_2\text{Fe}_4\text{As}_4\text{F}_2$. The self-fields at 10 and 15 K of both the pristine and proton irradiated samples are indicated by arrows.

Now, we show that α , which determines the field dependence of J_c ($\propto H^{-\alpha}$), can be overestimated in $\text{KCa}_2\text{Fe}_4\text{As}_4\text{F}_2$ due to a large and field-dependent $S(H)$. This is explained conceptually in Figure 6. When the magnetic field is applied and critical state is formed at $t = 0$, magnetic relaxation starts right after that. On the other hand, magnetization measurements for the evaluation of J_c are done after some time delay t . If $S(H)$ does not depend on a magnetic field, reduction of J_c , expressed by black arrows, is constant at all fields. In the case of $\text{KCa}_2\text{Fe}_4\text{As}_4\text{F}_2$ with a field-dependent $S(H)$ ($dS(H)/dH > 0$), however, reduction of J_c with time becomes larger at higher fields, as expressed by red arrows. Such an increased reduction of J_c at high fields makes apparent α larger, which may explain the relatively large α in $\text{KCa}_2\text{Fe}_4\text{As}_4\text{F}_2$.

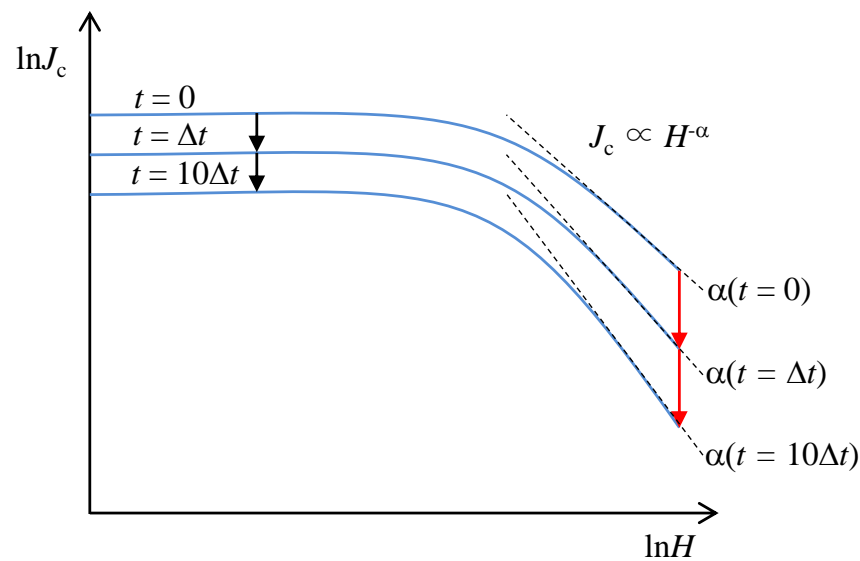


Figure 6. Schematic magnetic field dependence of J_c in a double logarithmic plot at different times after preparing the critical state at $t = 0$. When the normalized magnetic relaxation rate increases appreciably with the field, measured J_c values at high fields after some time delay ($t, 10t, \dots$) become smaller, resulting in stronger apparent magnetic field dependence of J_c , namely a larger α .

Next, we discuss the behavior of $S(H)$ in low and high magnetic fields. According to the collective creep theory, the H dependence of S is determined by the variation of the glassy exponent μ , as observed in $\text{YBa}_2\text{Cu}_3\text{O}_7$ [55]. In this theory, the glassy exponent (μ) is related to the vortex-bundle size [33]. In a three-dimensional system, it is predicted as $\mu = 1/7, 5/2, 7/9$ for single-vortex, small-bundle, and large-bundle regimes, respectively [33,56]. The collective creep theory is characterized by the J dependence of U . Collective creep theory, which considers vortex elasticity, predicts an inverse power law form for the energy barrier:

$$U(J) = U_0(J_{c0}/J)^\mu, \quad (2)$$

where J_{c0} is the temperature-dependent critical current density in the absence of flux creep, U_0 is the flux activation energy in the absence of flux creep, and $U(J)$ is flux activation energy [57]. This formula can be applied when relaxation process goes on and J is reduced ($J \ll J_{c0}$). On the other hand, at low temperatures and fields, the simple linear relationship proposed in the Anderson–Kim model [33], as shown below, is often accurate:

$$U(J) = U_0(1 - J_{c0}/J). \quad (3)$$

This model neglects vortex elasticity and vortex–vortex interactions. This relation is often limited to the early stages of the relaxation process ($J \sim J_{c0}$). To express behavior of $U(J)$ for a wide range of J , described by Equations (2) and (3), the interpolation formula is commonly used, as shown below [57]:

$$U(J) = \frac{U_0}{\mu} [(J_{c0}/J)^\mu - 1]. \quad (4)$$

On the other hand, from the Arrhenius relation, U can be also described as:

$$U = k_B T \ln(t/t_{\text{eff}}), \quad (5)$$

where k_B is the Boltzmann constant and t_{eff} is the effective hopping attempt time [34]. By combining Equations (4) and (5), time and temperature dependent $J(T, t)$ and S are given as follows [57]:

$$J(T, t) = \frac{J_{c0}}{[1 + (\mu k_B T / U_0) \ln(t / t_{\text{eff}})]^{1/\mu}} \quad (6)$$

$$S = \frac{k_B T}{U_0 + \mu k_B T \ln(t / t_{\text{eff}})}. \quad (7)$$

From this formula, we can observe that S is enhanced in the single vortex regime, where μ takes a relatively small value of $1/7$. On the other hand, the density of vortices is relatively sparse at fields below H_{sf} . In such a low-field regime, vortices may behave independently. So, one of the possible origins of the peak in $S(H)$ at low magnetic fields is the enhanced $S(H)$ with a smaller μ in the single vortex regime. It should be noted that, in the case of proton irradiated (Ba,K)Fe₂As₂, peaks in $S(H)$ disappear and only dip structures are observed, and α changes from $1/2$ to $1/3$ [27]. From these facts, enhancement of contribution of strong pinning by introducing point defects in (Ba,K)Fe₂As₂ is suggested [27]. On the other hand, the degree of suppression of S in KCa₂Fe₄As₄F₂ after proton irradiation is small and α is still larger than $1/2$. Comparing the effect of proton irradiation on $S(H)$ at low magnetic fields in these two materials, it is suggested that strong pinning nature of vortices in KCa₂Fe₄As₄F₂ is even more dominant after proton irradiation compared with that in (Ba,K)Fe₂As₂. This is consistent with the change of α from 1 to $1/2$, as discussed above. At high magnetic fields, $S(H)$ gradually increases with increasing H . As discussed above, one of possible explanations for the increase in $S(H)$ is gradual reduction of μ caused by the change in the vortex bundle size, from small bundles ($\mu = 5/2$) to large bundles ($\mu = 7/9$). Another possible origin of gradual increase in $S(H)$ with increase H is the significantly low H_{irr} in KCa₂Fe₄As₄F₂ originated from highly anisotropic crystal structure and resulting large anisotropy [12,16]. $S(H)$ is expected to diverge as H approaches H_{irr} , and H_{irr} is reduced with increasing temperature. So, the strong anisotropy in KCa₂Fe₄As₄F₂ significantly affects the behaviors of S at high temperatures and high magnetic fields. It should be pointed out that this $S(H)$ behavior affects the magnetic field dependence of J_c . At high magnetic fields and high temperatures, a simple power-law dependence of J_c on H is not observed and J_c decrease rapidly with increasing H as shown in Figure 4a–c. This is related to the rapid increase of $S(H)$ with increasing H , as discussed in Figure 6. After the proton irradiation, field dependences of both J_c and S become moderate, as shown in Figure 4b,c and Figure 5b. Although the true H_{irr} defined by the onset of nonlinearity in KCa₂Fe₄As₄F₂ may not be affected by the introduction of point defects, as reported in YBa₂Cu₃O₇ [31], the enhancement of pinning force by proton irradiation explains weaker field dependence of J_c and S .

Figure 7a,b show the temperature dependence of S at $H = 10, 20$, and 30 kOe for $H // c$ in the pristine and 3 MeV proton irradiated KCa₂Fe₄As₄F₂ at a dose of 3×10^{16} ions/cm², respectively. In both the pristine and proton irradiated samples, $S(T)$ shows a monotonic increase with increasing temperature without a plateau-like behavior, and the slope of $S(T)$ increases with increasing magnetic field. The temperature dependence of $S(T)$ becomes weaker only at 10 kOe between 10 K and 15 K. According to the collective creep theory, $S(T)$ is proportional to temperature at low temperatures, while it shows a plateau at intermediate T ($\gg U_0 / (k_B \ln(t / t_{\text{eff}}))$) with a value of $S = 0.02$ – 0.04 [58]. So, one may say that the behavior of $S(T)$ at 10 kOe in the above- T range can be explained in the framework of collective creep theory. However, the value of $S(T)$ between 10 K and 15 K is larger than the expected value. Plateau-like behaviors of $S(T)$ have been observed in, not only YBa₂Cu₃O₇ [58], but also in 122-type compounds with reasonable values of S of 0.01 – 0.04 [24,27]. However, with an increasing magnetic field, the weak temperature dependence of $S(T)$ between 10 K and 15 K disappears, and $S(T)$ strongly increases at higher temperatures. Low H_{irr} in anisotropic KCa₂Fe₄As₄F₂ can explain the stronger temperature dependence of $S(T)$ at high fields. On the other hand, such a divergent behavior of $S(T)$ at high temperatures is suppressed by proton irradiation, as shown in Figure 7b.

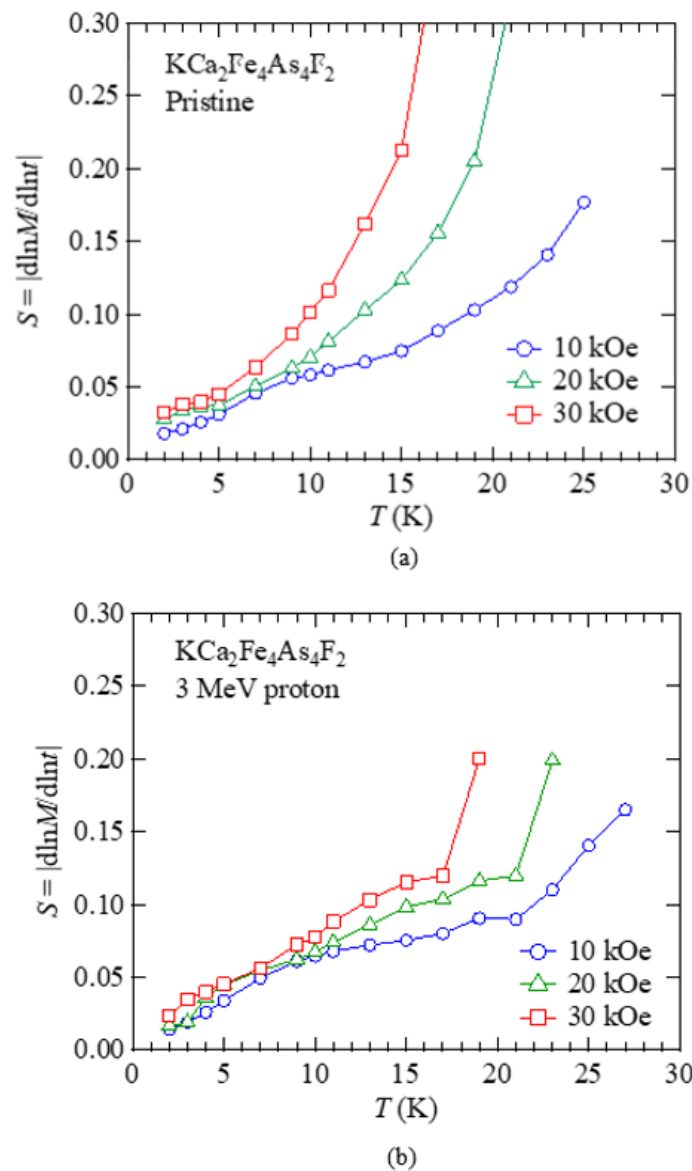


Figure 7. Temperature dependence of the normalized magnetic relaxation rate S at $H = 10, 20,$ and 30 kOe under $H//c$ in (a) the pristine and (b) 3 MeV proton irradiated (3×10^{16} ions/cm²) $\text{KCa}_2\text{Fe}_4\text{As}_4\text{F}_2$.

It is important to determine the value of μ in discussing vortex dynamics since μ includes information on the size of the vortex bundle in the collective creep theory. To extract this value, it is convenient to evaluate inverse current density dependence of effective pinning energy, U^* , which is defined as follows:

$$U^* = k_B T / S. \quad (8)$$

From this equation and “interpolation formula”, U^* can be calculated as:

$$U^* = U_0 + \mu k_B T \ln(t/t_{\text{eff}}) = U_0 (J_{c0}/J)^\mu. \quad (9)$$

Thus, the slope in the double logarithmic plot of U^* vs. $1/J$ gives the value of μ , as shown in Figure 8a,b. For this analysis, a proper choice of H is important to determine a region with a unique μ [27]. However, since power-law field dependence of J_c is broken down in $\text{KCa}_2\text{Fe}_4\text{As}_4\text{F}_2$, we chose a magnetic field of $H = 20$ kOe, where α is nearly constant below 15 K to avoid the effect of fast relaxation at high temperatures and at high

magnetic fields. In this way, we evaluated $\mu = 0.70$ and 0.22 for the pristine and proton irradiated $\text{KCa}_2\text{Fe}_4\text{As}_4\text{F}_2$, respectively. For comparison, we also plotted U^* vs. $1/J$ curves for the pristine and proton irradiated $(\text{Ba,K})\text{Fe}_2\text{As}_2$ in Figure 9a,b, respectively, using the data of relaxation analyses described in Ref. [27]. We evaluated $\mu = 0.82$ and 0.39 for the pristine and 3 MeV proton irradiated ($5.6 \times 10^{16} \text{ ions/cm}^2$) $(\text{Ba,K})\text{Fe}_2\text{As}_2$, respectively. Note that $\mu \sim 1$ in pristine crystal is often reported in $\text{YBa}_2\text{Cu}_3\text{O}_7$ [32] and IBSs [24,59]. After proton irradiation, however, μ becomes significantly smaller in both $\text{KCa}_2\text{Fe}_4\text{As}_4\text{F}_2$ and $(\text{Ba,K})\text{Fe}_2\text{As}_2$. This trend has also been reported in $\text{Ba}(\text{Fe,Co})_2\text{As}_2$ [24]. Values of μ in various IBSs are summarized in Table 1. The values of μ in most of pristine IBSs are ~ 1 , except for $\text{Li}_{0.8}\text{Fe}_{0.2}\text{OHFeSe}$. In $\text{Li}_{0.8}\text{Fe}_{0.2}\text{OHFeSe}$, a very large value of $\mu \sim 4.1$ was reported, although the anisotropy parameter is comparable to that in $\text{KCa}_2\text{Fe}_4\text{As}_4\text{F}_2$ [37]. It is discussed that the very large μ in $\text{Li}_{0.8}\text{Fe}_{0.2}\text{OHFeSe}$ may indicate that vortices in this material are in the crossover regime between elastic Abrikosov vortices to stacks of pancake vortices. The fact that the μ value in $\text{KCa}_2\text{Fe}_4\text{As}_4\text{F}_2$ was ~ 1 may suggest that vortices in this material were more like Abrikosov vortices, similar to the case of $(\text{Ba,K})\text{Fe}_2\text{As}_2$. On the other hand, negative slopes of U^* versus $1/J$ are also observed at small J . This negative slope is often denoted as p in the plastic creep scenario with $p \sim -0.5$ and is confirmed experimentally [60]. Evaluated $p = -0.25$ and -0.69 for pristine $\text{KCa}_2\text{Fe}_4\text{As}_4\text{F}_2$ and $(\text{Ba,K})\text{Fe}_2\text{As}_2$ are roughly consistent with this scenario. In the case of proton-irradiated $\text{KCa}_2\text{Fe}_4\text{As}_4\text{F}_2$, however, we were unable to access the negative slope region at a small J , while $p = -0.26$ was obtained in the proton-irradiated $(\text{Ba,K})\text{Fe}_2\text{As}_2$. Reduction of $|p|$ after introduction of point defects was also observed in $\text{Ba}(\text{Fe,Co})_2\text{As}_2$ [24]. Dose dependent measurements of vortex dynamics in the plastic region may shed light on the evolution of the plastic behavior.

Table 1. Glassy exponents for elastic creep μ in various IBS compounds, estimated from U^* vs. $1/J$ plots.

	$\text{KCa}_2\text{Fe}_4\text{As}_4\text{F}_2$	$(\text{Ba,K})\text{Fe}_2\text{As}_2$	$\text{Ba}(\text{Fe,Co})_2\text{As}_2$	$\text{Li}_{0.8}\text{Fe}_{0.2}\text{OHFeSe}$	$\text{Fe}(\text{Te,Se})$	FeSe
Pristine	0.70	0.82	1.09 [24]	4.1 [37]	1.34 [35]	0.71 [36]
Proton liubinirradiated	0.22	0.39	0.82 [24]	-	-	-

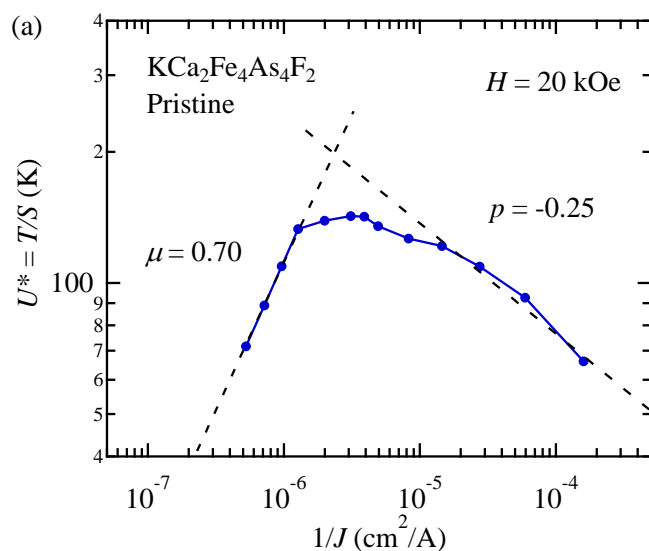


Figure 8. Cont.

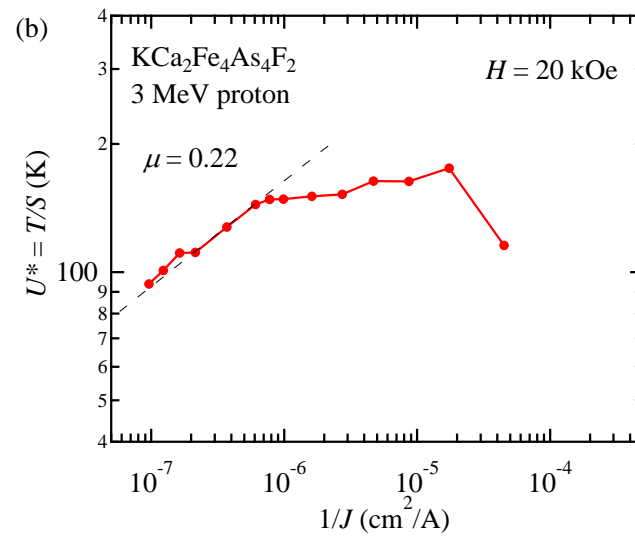


Figure 8. Inverse current density dependence of effective pinning energy U^* at $H = 20$ kOe in (a) the pristine and (b) 3 MeV proton irradiated (3×10^{16} ions/cm²) $\text{KCa}_2\text{Fe}_4\text{As}_4\text{F}_2$.

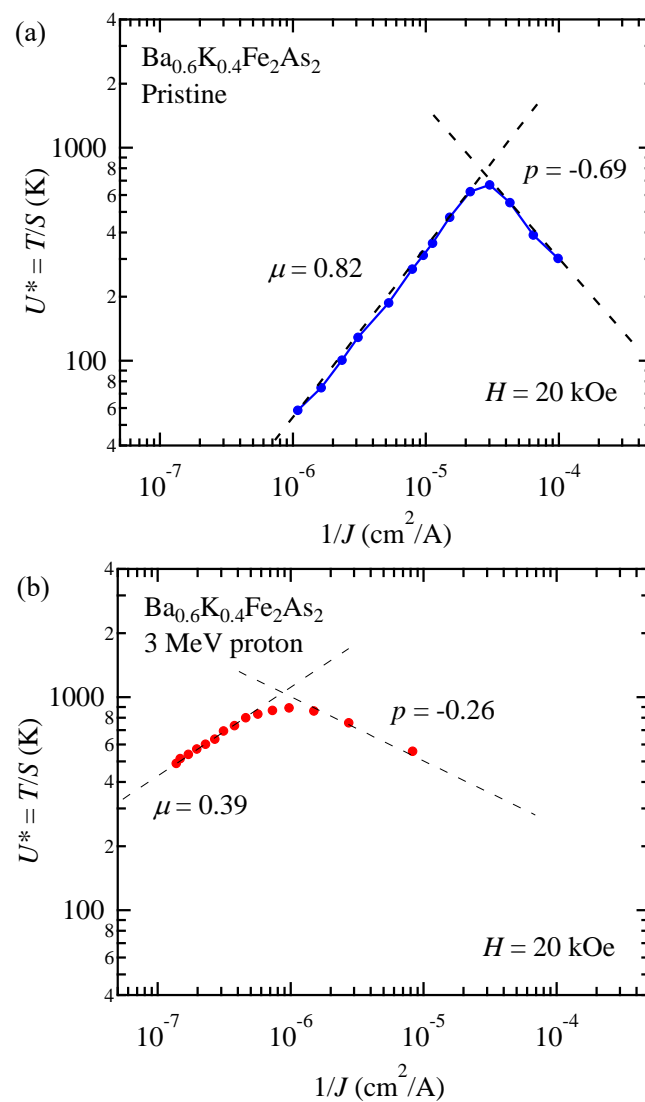


Figure 9. Inverse current density dependence of effective pinning energy U^* at 20 kOe in (a) the pristine and (b) 3 MeV proton irradiated (5.6×10^{16} ions/cm²) $(\text{Ba,K})\text{Fe}_2\text{As}_2$.

From the above experimental results and discussion, we can form a conjecture that predominant pinning in the pristine $\text{KCa}_2\text{Fe}_4\text{As}_4\text{F}_2$ is as follows. The large $J_c \sim 8 \text{ MA/cm}^2$ in the pristine sample is attributable to the embedded strong pinning centers, while artificial defects introduced by the irradiation enhance J_c to more than double. Vortex dynamics in $\text{KCa}_2\text{Fe}_4\text{As}_4\text{F}_2$ is similar to those in weakly anisotropic $(\text{Ba,K})\text{Fe}_2\text{As}_2$ rather than $\text{Li}_{0.8}\text{Fe}_{0.2}\text{OHFeSe}$ with similar anisotropy parameters. However, the effects of proton irradiation on magnetization, magnetic relaxation, and their behaviors at high temperatures and high magnetic fields are different from those in $(\text{Ba,K})\text{Fe}_2\text{As}_2$. Low H_{irr} in $\text{KCa}_2\text{Fe}_4\text{As}_4\text{F}_2$ due to large anisotropy causes a breakdown of clear power-law dependence of J_c on the magnetic field. Since the slope of $U^* - 1/J$ curve shows negative slope in a wide range of $1/J$ in the pristine sample, the effect of the plastic creep should be considered for the comprehensive understanding of the vortex dynamics in this system. The small value of H_{irr} and the large value of S , as well as the rapid decay of J_c-H at high temperatures and high magnetic fields, support this idea. We leave it as an open problem since the study on such fast dynamics is beyond the scope of this paper.

4. Summary

J_c and vortex pinning properties in $\text{KCa}_2\text{Fe}_4\text{As}_4\text{F}_2$ single crystals before and after introduction of artificial defects by ion irradiations are systematically studied. Columnar and point defects are introduced by 2.6-GeV U-ions and 3 MeV protons irradiations, respectively. The in-plane J_c evaluated from the measurement of irreversible magnetization at 2 K under the self-field is 8 MA/cm^2 , which is the largest among all IBSSs. J_c under self-field at 2 K is strongly enhanced up to 19.4 or 17.5 MA/cm^2 by irradiation of 2.6 GeV U-ions or 3 MeV protons, respectively. In both cases, suppression of T_c is observed. Quantitative differences of irradiation dose dependence of T_c compared with those of $(\text{Ba,K})\text{Fe}_2\text{As}_2$ can be explained by considering the presence of embedded defects in the pristine $\text{KCa}_2\text{Fe}_4\text{As}_4\text{F}_2$. Vortex dynamics in the pristine and proton irradiated $\text{KCa}_2\text{Fe}_4\text{As}_4\text{F}_2$ single crystals are also investigated from the analyses of field dependence of J_c and the normalized magnetic relaxation rate. The values of α from ~ 1 to $\sim 1/2$ before and after proton irradiation, and the behavior of S suggest that the vortex system in the pristine and proton irradiated $\text{KCa}_2\text{Fe}_4\text{As}_4\text{F}_2$ can be described by strong pinning. Vortex dynamics in $\text{KCa}_2\text{Fe}_4\text{As}_4\text{F}_2$ is similar to that in weakly anisotropic $(\text{Ba,K})\text{Fe}_2\text{As}_2$ rather than $\text{Li}_{0.8}\text{Fe}_{0.2}\text{OHFeSe}$ with similar anisotropy parameter. Low H_{irr} in $\text{KCa}_2\text{Fe}_4\text{As}_4\text{F}_2$ due to large anisotropy can explain some of unique behaviors of J_c such as break down of clear power-law dependence on the magnetic field.

Author Contributions: Conceptualization, methodology and validation, S.P., S.T. and T.T. (Tsuyoshi Tamegai); formal analysis, S.P., S.T., Y.K., T.T. (Toshihiro Taen) and A.I.; investigation, S.P., S.T., Y.K., A.T., W.L., T.T. (Toshihiro Taen), T.W., G.M. and A.I.; resources, T.W., G.M. and H.K.; data curation, S.P., S.T., Y.K., T.T. (Toshihiro Taen) and A.I.; writing—original draft preparation, S.P., S.T. and T.T. (Tsuyoshi Tamegai); writing—review and editing, S.P., S.T., T.T. (Toshihiro Taen) and T.T. (Tsuyoshi Tamegai); visualization, S.P., S.T. and T.T. (Toshihiro Taen); supervision, S.P. and T.T. (Tsuyoshi Tamegai); project administration, T.T. (Tsuyoshi Tamegai); funding acquisition, T.T. (Tsuyoshi Tamegai). All authors have read and agreed to the published version of the manuscript.

Funding: This work was partially supported by a Grant in Aid for Scientific Research (A) (17H01141) from the Japan Society for the Promotion of Science (JSPS).

Institutional Review Board Statement: Not applicable.

Informed Consent Statement: Not applicable.

Data Availability Statement: The data presented in this study are available on request from the corresponding author.

Acknowledgments: We are grateful to T. Kambara and A. Yoshida for helping U-ion irradiation, which is performed at RI Beam Factory operated by RIKEN Nishina Center and CNS, The University of Tokyo. We thank N. Ito and M. Morimoto for their help in sample preparation.

Conflicts of Interest: The authors declare no conflict of interest.

References

1. Stewart, G.R. Superconductivity in iron compounds. *Rev. Mod. Phys.* **2011**, *83*, 1589–1652. [[CrossRef](#)]
2. Rotter, M.; Tegel, M.; Johrendt, D. Superconductivity at 38 K in the Iron Arsenide $Ba_{1-x}K_xFe_2As_2$. *Phys. Rev. Lett.* **2008**, *101*, 107006. [[CrossRef](#)] [[PubMed](#)]
3. Tsuei, C.C.; Kirtley, J.R. Pairing symmetry in cuprate superconductors. *Rev. Mod. Phys.* **2000**, *72*, 969–1016. [[CrossRef](#)]
4. Tafuri, F.; Kirtley, J.R. Weak links in high critical temperature superconductors. *Rep. Prog. Phys.* **2000**, *68*, 2573–2663. [[CrossRef](#)]
5. Wang, Z.C.; He, C.Y.; Wu, S.Q.; Tang, Z.T.; Liu, Y.; Ablimit, A.; Feng, C.M.; Cao, G.H. Superconductivity in $KCa_2Fe_4As_4F_2$ with Separate Double Fe_2As_2 Layers. *J. Am. Chem. Soc.* **2016**, *138*, 7856–7859. [[CrossRef](#)] [[PubMed](#)]
6. Wang, Z.; He, C.; Tang, Z.; Wu, S.; Cao, G. Crystal structure and superconductivity at about 30 K in $ACa_2Fe_4As_4F_2$ ($A = Rb, Cs$). *Sci. China Mater.* **2017**, *60*, 83–89. [[CrossRef](#)]
7. Wang, Z.C.; He, C.Y.; Wu, S.Q.; Tang, Z.T.; Liu, Y.; Ablimit, A.; Tao, Q.; Feng, C.M.; Xu, Z.A.; Cao, G.H. Superconductivity at 35 K by self doping in $RbGd_2Fe_4As_4O_2$. *J. Phys. Condens. Matter* **2017**, *29*, 11LT01. [[CrossRef](#)]
8. Wang, Z.C.; He, C.Y.; Wu, S.Q.; Tang, Z.T.; Liu, Y.; Cao, G.H. Synthesis, Crystal Structure and Superconductivity in $RbLn_2Fe_4As_4O_2$ ($Ln = Sm, Tb, Dy, \text{ and } Ho$). *Chem. Mater.* **2017**, *29*, 1805–1812. [[CrossRef](#)]
9. Wu, S.Q.; Wang, Z.C.; He, C.Y.; Tang, Z.T.; Liu, Y.; Cao, G.H. Superconductivity at 33–37 K in $ALn_2Fe_4As_4O_2$ ($A = K \text{ and } Cs; Ln = \text{lanthanides}$). *Phys. Rev. Mater.* **2017**, *1*, 044804. [[CrossRef](#)]
10. Dong, X.; Jin, K.; Yuan, D.; Zhou, H.; Yuan, J.; Huang, Y.; Hua, W.; Sun, J.; Zheng, P.; Hu, W.; et al. $(Li_{0.84}Fe_{0.16})OHFe_{0.98}Se$ superconductor: Ion-exchange synthesis of large single-crystal and highly two-dimensional electron properties. *Phys. Rev. B* **2015**, *92*, 064515. [[CrossRef](#)]
11. Sun, S.; Wang, S.; Yu, R.; Lei, H. Extreme anisotropy and anomalous transport properties of heavily electron doped $Li_x(NH_3)_yFe_2Se_2$ single crystals. *Phys. Rev. B* **2017**, *96*, 064512. [[CrossRef](#)]
12. Wang, T.; Chu, J.; Jin, H.; Feng, J.; Wang, L.; Song, Y.; Zhang, C.; Xu, X.; Li, W.; Li, Z.; et al. Single-Crystal Growth and Extremely High H_{c2} of 12442-Type Fe-Based Superconductor $KCa_2Fe_4As_4F_2$. *J. Phys. Chem. C* **2019**, *123*, 13925–13929. [[CrossRef](#)]
13. Wang, Z.C.; Liu, Y.; Wu, S.Q.; Shao, Y.T.; Ren, Z.; Cao, G.H. Giant anisotropy in superconducting single crystals of $CsCa_2Fe_4As_4F_2$. *Phys. Rev. B* **2019**, *99*, 144501. [[CrossRef](#)]
14. Yu, A.B.; Wang, T.; Wu, Y.F.; Huang, Z.; Xiao, H.; Mu, G.; Hu, T. Probing superconducting anisotropy of single crystal $KCa_2Fe_4As_4F_2$ by magnetic torque measurements. *Phys. Rev. B* **2019**, *100*, 144505. [[CrossRef](#)]
15. Hong, W.; Song, L.; Liu, B.; Li, Z.; Zeng, Z.; Li, Y.; Wu, D.; Sui, Q.; Xie, T.; Danilkin, S.; et al. Neutron Spin Resonance in a Quasi-Two-Dimensional Iron-Based Superconductor. *Phys. Rev. Lett.* **2020**, *125*, 117002. [[CrossRef](#)]
16. Pyon, S.; Kobayashi, Y.; Takahashi, A.; Li, W.; Wang, T.; Mu, G.; Ichinose, A.; Kambara, T.; Yoshida, A.; Tamegai, T. Anisotropic physical properties and large critical current density in $KCa_2Fe_4As_4F_2$ single crystal. *Phys. Rev. Mater.* **2020**, *4*, 104801. [[CrossRef](#)]
17. Wang, T.; Zhang, C.; Xu, L.; Wang, J.; Jiang, S.; Zhu, Z.; Wang, Z.; Chu, J.; Feng, J.; Wang, L.; et al. Strong Pauli paramagnetic effect in the upper critical field of $KCa_2Fe_4As_4F_2$. *Sci. China Phys. Mech. Astron.* **2020**, *63*, 227412. [[CrossRef](#)]
18. Civale, L.; Marwick, A.D.; Worthington, T.K.; Kirk, M.A.; Thompson, J.R.; Krusin-Elbaum, L.; Sun, Y.; Clem, J.R.; Holtzberg, F. Vortex confinement by columnar defects in $YBa_2Cu_3O_7$ crystals: Enhanced pinning at high fields and temperatures. *Phys. Rev. Lett.* **1991**, *67*, 648–651. [[CrossRef](#)] [[PubMed](#)]
19. Krusin-Elbaum, L.; Civale, L.; Thompson, J.R.; Feild, C. Accommodation of vortices to columnar defects: Evidence for large entropic reduction of vortex localization. *Phys. Rev. B* **1996**, *53*, 11744–11750. [[CrossRef](#)]
20. Nakajima, Y.; Tsuchiya, Y.; Taen, T.; Tamegai, T.; Okayasu, S.; Sasase, M. Enhancement of critical current density in Co-doped $BaFe_2As_2$ with columnar defects introduced by heavy-ion irradiation. *Phys. Rev. B* **2009**, *80*, 012510. [[CrossRef](#)]
21. Prozorov, R.; Tanatar, M.A.; Roy, B.; Ni, N.; Bud'ko, S.L.; Canfield, P.C.; Hua, J.; Welp, U.; Kwok, W.K. Magneto-optical study of $Ba(Fe_{1-x}M_x)_2As_2$ ($M = Co \text{ and } Ni$) single crystals irradiated with heavy ions. *Phys. Rev. B* **2010**, *81*, 094509. [[CrossRef](#)]
22. Tamegai, T.; Taen, T.; Yagyuda, H.; Tsuchiya, Y.; Mohan, S.; Taniguchi, T.; Nakajima, Y.; Okayasu, S.; Sasase, M.; Kitamura, H.; et al. Effects of particle irradiations on vortex states in iron-based superconductors. *Supercond. Sci. Technol.* **2012**, *25*, 084008. [[CrossRef](#)]
23. Fang, L.; Jia, Y.; Chaparro, C.; Sheet, G.; Claus, H.; Kirk, M.A.; Koshelev, A.E.; Welp, U.; Crabtree, G.W.; Kwok, W.K.; et al. High, magnetic field independent critical currents in $(Ba,K)Fe_2As_2$ crystals. *Appl. Phys. Lett.* **2012**, *101*, 012601. [[CrossRef](#)]
24. Taen, T.; Nakajima, Y.; Tamegai, T.; Kitamura, H. Enhancement of critical current density and vortex activation energy in proton-irradiated Co-doped $BaFe_2As_2$. *Phys. Rev. B* **2012**, *86*, 094527. [[CrossRef](#)]
25. Kihlstrom, K.J.; Fang, L.; Jia, Y.; Shen, B.; Koshelev, A.E.; Welp, U.; Crabtree, G.W.; Kwok, W.K.; Kayani, A.; Zhu, S.F.; et al. High-field critical current enhancement by irradiation induced correlated and random defects in $(Ba_{0.6}K_{0.4})Fe_2As_2$. *Appl. Phys. Lett.* **2013**, *103*, 202601. [[CrossRef](#)]
26. Ohtake, F.; Taen, T.; Pyon, S.; Tamegai, T.; Okayasu, S.; Kambara, T.; Kitamura, H. Effects of heavy-ion irradiations in K-doped $BaFe_2As_2$. *Phys. C* **2015**, *518*, 47–50. [[CrossRef](#)]
27. Taen, T.; Ohtake, F.; Pyon, S.; Tamegai, T.; Kitamura, H. Critical current density and vortex dynamics in pristine and proton-irradiated $Ba_{0.6}K_{0.4}Fe_2As_2$. *Supercond. Sci. Technol.* **2015**, *28*, 085003. [[CrossRef](#)]

28. Haberkorn, N.; Kim, J.; Gofryk, K.; Ronning, F.; Sefat, A.S.; Fang, L.; Welp, U.; Kwok, W.K.; Civale, L. Enhancement of the critical current density by increasing the collective pinning energy in heavy ion irradiated Co-doped BaFe₂As₂ single crystals. *Supercond. Sci. Technol.* **2015**, *28*, 055011. [[CrossRef](#)]
29. Sun, Y.; Park, A.; Pyon, S.; Tamegai, T.; Kambara, T.; Ichinose, A. Effects of heavy-ion irradiation on FeSe. *Phys. Rev. B* **2017**, *95*, 104514. [[CrossRef](#)]
30. Torsello, D.; Gerbaldo, R.; Gozzelino, L.; Laviano, F.; Takahashi, A.; Park, A.; Pyon, S.; Ichinose, A.; Tamegai, T.; Ghigo, G. Twofold role of columnar defects in iron based superconductors. *Supercond. Sci. Technol.* **2020**, *33*, 094012. [[CrossRef](#)]
31. Civale, L.; Marwick, A.D.; McElfresh, M.W.; Worthington, T.K.; Malozemoff, A.P.; Holtzberg, F.H.; Thompson, J.R.; Kirk, M.A. Defect Independence of the Irreversibility Line in Proton Irradiated Y-Ba-Cu-O Crystals. *Phys. Rev. Lett.* **1990**, *65*, 1164–1167. [[CrossRef](#)]
32. Thompson, J.R.; Sun, Y.R.; Civale, L.; Malozemoff, A.P.; McElfresh, M.W.; Marwick, A.D.; Holtzberg, F. Effect of flux creep on the temperature dependence of the current density in Y-Ba-Cu-O crystals. *Phys. Rev. B* **1993**, *47*, 14440–14447. [[CrossRef](#)]
33. Blatter, G.; Feigel'man, M.V.; Geshkenbein, V.B.; Larkin, A.I.; Vinokur, V.M. Vortices in high-temperature superconductors. *Rev. Mod. Phys.* **1994**, *66*, 1125–1388. [[CrossRef](#)]
34. Yeshurun, Y.; Malozemoff, A.P.; Shaulov, A. Magnetic relaxation in high-temperature superconductors. *Rev. Mod. Phys.* **1996**, *68*, 911–949. [[CrossRef](#)]
35. Sun, Y.; Taen, T.; Tsuchiya, Y.; Pyon, S.; Shi, Z.; Tamegai, T. Magnetic relaxation and collective vortex creep in FeTe_{0.6}Se_{0.4} single crystal. *EPL* **2013**, *103*, 57013. [[CrossRef](#)]
36. Sun, Y.; Pyon, S.; Tamegai, T.; Kobayashi, R.; Watahige, T.; Kasahara, S.; Matsuda, Y.; Shibauchi, T. Critical current density, vortex dynamics, and phase diagram of single-crystal FeSe. *Phys. Rev. B* **2015**, *92*, 144509. [[CrossRef](#)]
37. Sun, Y.; Pyon, S.; Yang, R.; Qiu, X.; Feng, J.; Shi, Z.; Tamegai, T. Deviation from Canonical Collective Creep Behavior in Li_{0.8}Fe_{0.2}OHFeSe. *J. Phys. Soc. Jpn.* **2019**, *88*, 034703. [[CrossRef](#)]
38. Takahashi, A.; Pyon, S.; Kambara, T.; Yoshida, A.; Tamegai, T. Effects of Asymmetric Splayed Columnar Defects on the Anomalous Peak Effect in Ba_{0.6}K_{0.4}Fe₂As₂. *J. Phys. Soc. Jpn.* **2020**, *89*, 094705. [[CrossRef](#)]
39. Ito, N.; Pyon, S.; Kambara, T.; Yoshida, A.; Okayasu, S.; Ichinose, A.; Tamegai, T. Anisotropy of critical current densities in Ba_{1-x}K_xFe₂As₂ and Ba(Fe_{1-x}Co_x)₂As₂ with splayed columnar defects. *J. Phys. Conf. Ser.* **2018**, *1054*, 012020. [[CrossRef](#)]
40. Abrikosov, A.A.; Gor'kov, L.P. Contribution to the theory of superconducting alloys with paramagnetic impurities. *Sov. Phys. JETP* **1961**, *12*, 1243–1263.
41. Bean, C.P. Magnetization of high-field superconductors. *Rev. Mod. Phys.* **1964**, *36*, 31–39. [[CrossRef](#)]
42. Gyorgy, E.M.; van Dover, R.B.; Jackson, K.A.; Schneemeyer, L.F.; Waszczak, J.V. Anisotropic critical currents in Ba₂YC₃O₇ analyzed using an extended Bean model. *Appl. Phys. Lett.* **1989**, *55*, 283–285. [[CrossRef](#)]
43. Taen, T.; Ohtake, F.; Akiyama, H.; Inoue, H.; Sun, Y.; Pyon, S.; Tamegai, T.; Kitamura, H. Pair-breaking effects induced by 3-MeV proton irradiation in Ba_{1-x}K_xFe₂As₂. *Phys. Rev. B* **2013**, *88*, 224514. [[CrossRef](#)]
44. Hosono, H.; Yamamoto, A.; Hiramatsu, H.; Ma, Y. Recent advances in iron-based superconductors toward applications. *Mater. Today* **2018**, *21*, 278–302. [[CrossRef](#)]
45. Pyon, S.; Suwa, T.; Tamegai, T.; Takano, K.; Kajitani, H.; Koizumi, N.; Awaji, S.; Zhou, N.; Shi, Z. Improvements of fabrication processes and enhancement of critical current densities in (Ba,K)Fe₂As₂ HIP wires and tapes. *Supercond. Sci. Technol.* **2018**, *31*, 055016. [[CrossRef](#)]
46. Pyon, S.; Mori, H.; Tamegai, T.; Awaji, S.; Kito, H.; Ishida, S.; Yoshida, Y.; Kajitani, H.; Koizumi, N. Fabrication of small superconducting coils using (Ba,A)Fe₂As₂ (A: Na, K) round wires with large critical current densities. *Supercond. Sci. Technol.* **2021**, *34*, 105008. [[CrossRef](#)]
47. Van der Beek, C.J.; Konczykowski, M.; Kasahara, S.; Terashima, T.; Okazaki, R.; Shibauchi, T.; Matsuda, Y. Quasiparticle scattering induced by charge doping of iron-pnictide superconductors probed by collective vortex pinning. *Phys. Rev. Lett.* **2010**, *105*, 267002. [[CrossRef](#)]
48. Van der Beek, C.J.; Konczykowski, M.; Abal'oshev, A.; Abal'osheva, I.; Gierlowski, P.; Lewandowski, S.J.; Indenbom, M.V.; Barbanera, S. Strong pinning in high-temperature superconducting films. *Phys. Rev. B* **2002**, *66*, 024523. [[CrossRef](#)]
49. Brandt, E.H. The flux-line lattice in superconductors. *Rep. Prog. Phys.* **1995**, *58*, 1465–1594. [[CrossRef](#)]
50. Prischepal, S.L.; Montemurro, D.; Cirillo, C.; Attanasio, C.; Salvato, M.; Merlo, V.; Lykov, A.N.; Tsvetkov, A.Y. Thickness dependence of pinning mechanisms in granular Nb thin films. *Supercond. Sci. Technol.* **2006**, *19*, 1124–1129. [[CrossRef](#)]
51. Ovchinnikov, Y.N.; Ivlev, B.I. Pinning in layered inhomogeneous superconductors. *Phys. Rev. B* **1991**, *43*, 8024–8029. [[CrossRef](#)] [[PubMed](#)]
52. Park, A.; Mine, A.; Yamada, T.; Ohtake, F.; Akiyama, H.; Sun, Y.; Pyon, S.; Tamegai, T.; Kitahama, Y.; Mizukami, T.; et al. Enhancement of critical current density in a Ca_{0.85}La_{0.15}Fe(As_{0.92}Sb_{0.08})₂ superconductor with T_c = 47 K through 3 MeV proton irradiation. *Supercond. Sci. Technol.* **2016**, *29*, 055006. [[CrossRef](#)]
53. Park, A.; Veshchunov, I.; Mine, A.; Pyon, S.; Tamegai, T.; Kitamura, H. Effects of 6 MeV proton irradiation on the vortex ensemble in BaFe₂(As_{0.67}P_{0.33})₂ revealed through magnetization measurements and real-space vortex imaging. *Phys. Rev. B* **2020**, *101*, 224507. [[CrossRef](#)]
54. Tamegai, T.; Sato, M.; Yamamoto, T.; Ooi, S.; Shibauchi, T. Dimensional crossover of quantum collective creep in Bi₂Sr₂CaCu₂O_{8+y}. *Czechoslov. J. Phys.* **1996**, *46*, 1733–1734. [[CrossRef](#)]

55. Krusin-Elbaum, L.; Civale, L.; Vinokur, V.M.; Holtzberg, F. "Phase diagram" of the vortex-solid phase in Y-Ba-Cu-O crystals: A crossover from single-vortex (1D) to collective (3D) pinning regimes. *Phys. Rev. Lett.* **1992**, *69*, 2280–2283. [[CrossRef](#)]
56. Feigel'man, M.V.; Geshkenbein, V.B.; Larkin, A.I.; Vinokur, V.M. Theory of collective flux creep. *Phys. Rev. Lett.* **1989**, *63*, 2303–2306. [[CrossRef](#)]
57. Eley, S.; Willa, R.; Chan, M.K.; Bauer, E.D.; Civale, L. Vortex phases and glassy dynamics in the highly anisotropic superconductor HgBa₂CuO_{4+δ}. *Sci. Rep.* **2020**, *10*, 10239. [[CrossRef](#)]
58. Malozemoff, A.P.; Fisher, M.P.A. Universality in the current decay and flux creep of Y-Ba-Cu-O high-temperature superconductors. *Phys. Rev. B* **1990**, *42*, 6784–6786. [[CrossRef](#)]
59. Salem-Sugui, S.; Ghivelder, L.; Alvarenga, A.D.; Cohen, L.F.; Yates, K.A.; Morrison, K.; Pimentel, J.L.; Luo, H.; Wang, Z.; Wen, H.H. Flux dynamics associated with the second magnetization peak in the iron pnictide Ba_{1-x}K_xFe₂As₂. *Phys. Rev. B* **2010**, *82*, 054513. [[CrossRef](#)]
60. Abulafia, Y.; Shaulov, A.; Wolfus, Y.; Prozorov, R.; Burlachkov, L.; Yeshurun, Y.; Majer, D.; Zeldov, E.; Wühl, H.; Geshkenbein, V.B.; et al. Plastic Vortex Creep in YBa₂Cu₃O_{7-x} Crystals. *Phys. Rev. Lett.* **1996**, *77*, 1596–1599. [[CrossRef](#)]